

Evolution of LMC/M33-mass dwarf galaxies in the EAGLE simulation

Shi Shao^{1*}, Marius Cautun¹, Alis J. Deason¹, Carlos S. Frenk¹ and Tom Theuns¹

¹*Institute for Computational Cosmology, Department of Physics, Durham University, South Road Durham DH1 3LE, UK*

29 June 2018

ABSTRACT

We investigate the population of dwarf galaxies with stellar masses similar to the Large Magellanic Cloud (LMC) and M33 in the EAGLE galaxy formation simulation. In the field, galaxies reside in haloes with stellar-to-halo mass ratios of $1.03^{+0.50}_{-0.31} \times 10^{-2}$ (68% confidence level); systems like the LMC, which have an SMC-mass satellite, reside in haloes about 1.3 times more massive, which suggests an LMC halo mass at infall, $M_{200} = 3.4^{+1.8}_{-1.2} \times 10^{11} M_{\odot}$ (68% confidence level). The colour distribution of dwarfs is bimodal, with the red galaxies ($g - r > 0.6$) being mostly satellites. The fraction of red LMC-mass dwarfs is 15% for centrals, and for satellites this fraction increases rapidly with host mass: from 10% for satellites of Milky Way (MW)-mass haloes to nearly 90% for satellites of groups and clusters. The quenching timescale, defined as the time after infall when half of the satellites have acquired red colours, decreases with host mass from >5 Gyrs for MW-mass hosts to 2.5 Gyrs for cluster mass hosts. The satellites of MW-mass haloes have higher star formation rates and bluer colours than field galaxies. This is due to enhanced star formation triggered by gas compression shortly after accretion. Both the LMC and M33 have enhanced recent star formation that could be a manifestation of this process. After infall into their MW-mass hosts, the $g - r$ colours of LMC-mass dwarfs become bluer for the first 2 Gyrs, after which they rapidly redden. LMC-mass dwarfs fell into their MW-mass hosts only relatively recently, with more than half having an infall time of less than 3.5 Gyrs.

Key words: methods: numerical – galaxies: haloes – galaxies: kinematics and dynamics – galaxies: dwarfs – Magellanic Clouds

1 INTRODUCTION

Of the multitude of galaxies in the cosmos, dwarf galaxies are the most abundant and, at the same time, amongst the least understood. Galaxy formation is a complex process and even more so in the case of dwarf galaxies. For example, in the standard cosmological model, only a small fraction of low mass haloes are occupied by galaxies. Even for those that have a luminous counterpart, the relation between galaxy and dark matter halo properties is an intricate one, which is shaped by a diverse set of feedback processes (see e.g. the review of [Benson 2010](#)). Here, we focus on LMC-mass galaxies (i.e. the most massive dwarfs) and study their properties in the EAGLE cosmological simulation ([Schaye et al. 2015](#); [Crain et al. 2015](#)), which resolves a large number of such objects. These can be readily compared to observations, where LMC-mass dwarfs can be studied out to relatively large cosmological scales in a variety of environments (e.g. [Woods & Geller 2007](#); [Pozzetti et al. 2010](#); [Tollerud et al. 2011](#); [Geha et al. 2012](#); [Bauer et al. 2013](#)). Furthermore, the study of LMC-mass galaxies is key for understanding the formation history of the LMC and M33, the brightest satellites of the Milky Way (MW) and M31, respectively.

LMC-mass galaxies reside in relatively low mass haloes, of typical mass a few times $10^{11} M_{\odot}$ ([Moster et al. 2010](#); [Guo et al. 2010](#)), and have a diversity of colours and star formation rates (SFR). Large redshift surveys, such as the Sloan Digital Sky Survey (SDSS), have revealed that LMC-mass dwarfs have a bimodal $g - r$ colour distribution, forming an extended blue cloud and a narrower red sequence ([Strateva et al. 2001](#)). The fraction of red dwarfs varies with environment: LMC-mass field galaxies are significantly bluer than similar mass satellites ([Tollerud et al. 2011](#)). The same trend is seen in the star formation of LMC-mass galaxies, with overdense regions having a larger fraction of quiescent dwarfs ([Wijesinghe et al. 2012](#)). The trend in the fraction of red and quiescent galaxies with environment is a manifestation of quenching processes, such as ram pressure stripping and starvation, that typically act when galaxies reside in dense environments or become satellites of a more massive galaxy (e.g. [Blanton & Moustakas 2009](#), for a review; [Wetzel et al. 2013](#); [Fillingham et al. 2016](#); [Bahé et al. 2017](#); [Simpson et al. 2018](#); [Fattahi et al. 2018](#)).

Intriguingly, the LMC-mass satellites of the MW and M31, the LMC and M33 respectively, have very blue colours and are actively forming stars ([Muñoz-Mateos et al. 2007](#); [Harris & Zaritsky 2009](#); [Eskew & Zaritsky 2011](#); [Tollerud et al. 2011](#)). For example, the LMC is unusually blue; it lies in the $\sim 1\%$ tail of the

* E-mail: shi.shao@durham.ac.uk

SDSS $g - r$ colour distribution of galaxies of the same magnitude (Tollerud et al. 2011), and is forming more stars than expected on average for its stellar mass. This seems contrary to the average expectation that satellite galaxies should have redder colours and lower SFR, and raises the question of how efficient are MW-mass haloes at quenching their brightest satellites. The orbital dynamics of the LMC and M33 suggest that both these satellites were accreted recently, typically less than 2 Gyrs ago, and are on their first orbit around their central galaxies (Kallivayalil et al. 2006, 2013; Deason et al. 2015; Patel et al. 2017; Laporte et al. 2018; Cautun et al. 2018). Furthermore, SDSS observations find that the fraction of red satellites decreases with host halo mass and, for MW-mass host haloes, the blue satellites become more numerous than the red satellites (e.g. Weinmann et al. 2006; Kimm et al. 2009; Guo et al. 2013; Wang & et al., 2014). Typically, theoretical models fail to reproduce this trend, although Sales et al. (2015) have found a good agreement between observations and the galaxy population of the ILLUSTRIS hydrodynamic simulation.

The LMC and M33 are peculiar in another respect: only a small fraction of MW-mass systems are expected to host such bright satellites. Observationally, studies of MW-like galaxies in the SDSS (Liu et al. 2011; Guo et al. 2011; Tollerud et al. 2011; Wang & White 2012; Guo et al. 2013) and in the Galaxy And Mass Assembly (GAMA; Robotham et al. 2012) surveys have found that only about 10% have satellites as bright as the LMC. Systems that additionally have a Small Magellanic Cloud (SMC), which observations suggest fell into the MW as a satellite of the LMC (Kallivayalil et al. 2013, and discussion within), are even more rare. This result is confirmed by numerical simulations, which also show that the probability of having an LMC satellite varies strongly with host halo mass (e.g. Boylan-Kolchin et al. 2010; Busha et al. 2011).

The importance of the LMC, and possibly M33, is also reflected in the “satellites-of-satellites” population, which are dragged into the MW by more massive dwarfs. For example, the SMC, and potentially a large fraction of the dwarfs recently discovered by the Dark Energy Survey (DES) (Jethwa et al. 2016; Sales & et al., 2017), were likely satellites of the LMC. Due to its large total mass, with current estimates suggesting a total halo mass of $2.5 \times 10^{11} M_{\odot}$ (Peñarrubia et al. 2016; Cautun et al. 2018), the LMC is expected to have contributed up to 30% of the current MW satellite population (Deason et al. 2015; Shao et al. 2018).

In this paper, we study the properties of a large sample of LMC-mass galaxies in the EAGLE galaxy formation simulation. EAGLE is ideal for this study since it reproduces a range of key observables, such as the galaxy stellar mass function, cosmic star formation history, and galaxy sizes, metallicities, gas fractions and morphologies across a wide range of masses and different redshifts (Furlong et al. 2015; Lagos et al. 2015; Schaye et al. 2015; Trayford et al. 2015). LMC-mass dwarfs are resolved in EAGLE with about 1000 or more star particles, which allows for a robust characterization of their morphology, SFR and colour distribution. We probe how these properties vary according to environment, i.e. field versus satellite galaxies, and, in particular, we focus on LMC-mass satellites in MW-mass host haloes, with the goal of interpreting the observed properties and evolution of the LMC and M33.

The paper is organized as follows. Section 2 reviews the simulations used in this work and describes our sample selection; Section 3 presents our results on the statistics of field and satellite LMC-mass dwarfs; Section 4 discusses the implications of our findings in the context of LMC-like satellites of MW-mass haloes; we conclude with a short summary and discussion in Section 5.

2 SIMULATIONS AND METHODS

We make use of the main cosmological hydrodynamical simulation (labelled Ref-L0100N1504) performed as part of the EAGLE project (Schaye et al. 2015; Crain et al. 2015). Using a periodic cube of 100 Mpc side length, EAGLE follows the evolution of 1504^3 dark matter particles, and an initially equal number of gas particles. The dark matter particle mass is $9.7 \times 10^6 M_{\odot}$, and the initial gas particle mass is $1.8 \times 10^6 M_{\odot}$. EAGLE uses a *Planck* cosmology (Planck Collaboration XVI 2014) with cosmological parameters: $\Omega_{\text{m}} = 0.307$, $\Omega_{\text{b}} = 0.04825$, $\Omega_{\Lambda} = 0.693$, $h = 0.6777$, $\sigma_8 = 0.8288$ and $n_{\text{s}} = 0.9611$.

The simulation was performed using a modified version of the GADGET code (Springel 2005), which includes state-of-the-art smoothed particle hydrodynamics methods (Dalla Vecchia & Schaye 2012; Hopkins 2013; Schaller et al. 2015). The baryonic physics implementation accounts for a multitude of processes relevant to galaxy formation, such as element-by-element cooling using the Wiersma et al. (2009a) prescription, stochastic star formation with a metallicity dependent threshold (Schaye 2004), thermal energy feedback associated with star formation (Dalla Vecchia & Schaye 2012), and the injection of hydrogen, helium and metals into the interstellar medium from supernovae and stellar mass loss (Wiersma et al. 2009b). Each star particle corresponds to a single stellar population with a Chabrier (2003) initial mass function. Supermassive black holes grow through mergers and accretion of low angular momentum material (Springel et al. 2005; Rosas-Guevara et al. 2015; Schaye et al. 2015) and, in the process, inject thermal energy into the surrounding gas (Booth & Schaye 2009; Dalla Vecchia & Schaye 2012). The EAGLE subgrid models were calibrated to reproduce three present day observables (Crain et al. 2015; Schaye et al. 2015): the stellar mass function, the distribution of galaxy sizes, and the relation between supermassive black hole mass and host galaxy mass. For a more detailed description, we refer the reader to Schaye et al. (2015).

We make use of the $z = 0$ EAGLE halo and galaxy catalogue (McAlpine et al. 2016). Haloes are initially identified using the friends-of-friends (FOF; Davis et al. 1985) algorithm with a linking length 0.2 times the mean interparticle separation. The resulting FOF groups were further split into gravitationally bound substructures using the SUBFIND code (Springel et al. 2001; Dolag et al. 2009), which was applied to the full matter distribution (dark matter, gas and stars) associated with each FOF group. The main halo is determined by the subhalo that contains the most bound particle, while the remaining subhaloes are classified as satellites. The stellar distribution associated with the main subhalo is identified as the central galaxy. The main haloes are characterized by the mass, M_{200} , and radius, R_{200} , that define an enclosed spherical overdensity of 200 times the critical density. The position of each galaxy, for both centrals and satellites, is given by their most bound particle.

Fig. 1 presents the relation in EAGLE between the stellar masses of central galaxies and the mass of their host haloes. We do not show satellites since their subhalo mass, which SUBFIND defines as the bound mass within the tidal radius, varies depending on the position of the object along its orbit. The figure shows that the stellar and halo masses are correlated, albeit with a large scatter. The scatter, while small at large masses, increases significantly for low mass haloes.

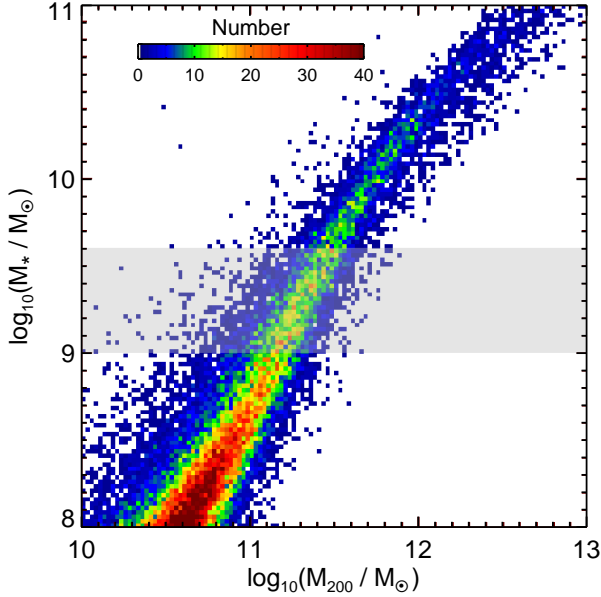


Figure 1. The relation between stellar mass, M_* , and total halo mass, M_{200} , for central galaxies in the EAGLE simulation. The colours indicate the number of galaxies in each halo and stellar mass bin (see legend). The grey shaded region shows galaxies with stellar masses in the range $1 - 4 \times 10^9 M_\odot$, which corresponds to our sample of field LMC-mass dwarfs (we also select LMC-mass satellites, which are not shown in this diagram).

2.1 Sample selection

We select LMC-mass dwarfs by requiring that they have a stellar mass in the range, $M_* \in [1, 4] \times 10^9 M_\odot$, which is motivated by the following. First, due to uncertainties in the stellar mass to light ratio, the LMC stellar mass is somewhat uncertain, with mass estimates spanning the range $1.5 - 2.7 \times 10^9 M_\odot$ (e.g. van der Marel & et al., 2002; McConnachie 2012). Secondly, to have good statistics we need a large sample of LMC-mass dwarfs, and thus a mass range as wide as possible. A typical LMC-mass dwarf in EAGLE is resolved with a thousand or more star particles and with hundreds of gas particles, which allows for a robust quantification of its present day properties as well as its formation history.

We split our LMC-mass dwarfs into two categories: (1) the satellite galaxy sample, which consists of LMC-mass dwarfs within a radius, R_{50} , from a more massive halo, and (2) the field galaxy sample, which comprises central galaxies that are not within distance R_{50} from a more massive halo. The R_{50} radius defines an enclosed spherical overdensity of 50 times the critical density (it is approximately $2^{2/3} \times R_{200}$). We choose this bounding radius because MW studies typically take 300 kpc as the Galactic halo radius, which for a MW halo mass of $10^{12} M_\odot$, corresponds to R_{50} . In EAGLE, we find 3774 field¹ galaxies and 2551 satellite galaxies. The sample of field LMC-mass dwarfs is highlighted in Fig. 1 using a grey shaded region, which corresponds to the stellar mass selection criteria.

We further select a subset of LMC-mass satellites that reside in MW-mass haloes, which we define as any host halo with a mass in the range, $M_{200} \in [0.5, 2] \times 10^{12} M_\odot$ (Cautun et al. 2014; Wang et al. 2015; Peñarrubia et al. 2016). We find 381 LMC-mass

¹ We use the term “field” to refer to galaxies that are not satellites of other galaxies.

dwarfs within R_{50} of our MW-mass halo sample, with the MW-mass hosts having a median halo mass $\approx 1.0 \times 10^{12} M_\odot$ and a median $R_{50} \approx 313$ kpc.

To study the evolution of LMC-mass satellites, we make use of the EAGLE snapshots, which are finely spaced (about every 70 Myrs) simulation outputs that allow us to trace the orbits of satellites with very good time resolution. We define the infall time for each dwarf as the time when it first crosses R_{50} of the progenitor of its $z = 0$ host halo.

2.2 Galaxy morphology and colour

To quantify the morphology of LMC-mass dwarfs, we divide the stellar mass of galaxies into two components: spheroid and disc, which we identify using the procedure of Abadi et al. (2003, see also Scannapieco & et al., 2009; Crain et al. 2010; Sales et al. 2012). We calculate the circularity parameter of each star, $\epsilon = j_z / j_{\text{circ}}(E)$, defined as the ratio between the component of the specific angular momentum perpendicular to the disc, j_z , and that for a circular orbit with the same total energy, $j_{\text{circ}}(E)$. The disc direction is given by the angular momentum of all the star particles within twice the half stellar mass radius, r_h . If we assume that the spheroidal component of each galaxy is fully velocity dispersion dominated, then the bulge mass corresponds to twice the mass of the stars with $\epsilon < 0$. Note that $\epsilon < 0$ corresponds to counter-rotating stars, i.e. stars for which the scalar product between the stars’ angular momentum and that of the disc is negative.

We take the galaxy colours calculated by Trayford et al. (2015), which are based on the GALAXEV population synthesis models of Bruzual & Charlot (2003). The colours are estimated by modelling the stellar populations of EAGLE star particles, which represent a simple stellar population with a Chabrier (2003) initial mass function, taking into account their ages and metallicities. The galaxy spectra were summed over all the stellar particles within a spherical aperture of 30 kpc and convolved with the colour filter response function. Here, we take the colour of each galaxy from the intrinsic $g - r$ colour without dust extinction. Trayford et al. showed that these colours are in broad agreement with observational data and that, in particular, EAGLE produces a red sequence of passive galaxies and a blue cloud of star-forming galaxies.

3 GENERAL PROPERTIES OF LMC-MASS DWARFS

We now study general properties, such as halo mass, morphology, colour and star formation rate (SFR) of LMC-mass dwarf galaxies. In particular, we focus on differences between the populations of field dwarfs and satellite galaxies, with emphasis on satellites around MW-mass host haloes.

3.1 Halo mass

We start by characterizing the EAGLE haloes that host the LMC-mass dwarfs. From Fig. 1, we find that the typical field LMC-mass galaxy resides in a halo with a total mass of $\sim 2 \times 10^{11} M_\odot$, but the relation is characterized by significant scatter. Most striking are the handful of objects with the same stellar mass as the LMC which reside in a few $\times 10^{10} M_\odot$ mass haloes. These are not satellites, since Fig. 1 shows only central LMC-mass dwarfs, and are likely “backsplash” galaxies which were, at least for some period of time, satellites around more massive host haloes and thus were tidally stripped (Moore et al. 2004). We have checked that all the LMC-mass dwarfs residing in haloes with $M_{200} < 10^{10.5} M_\odot$ are back-splash galaxies. The scatter in the stellar-to-halo mass relation for

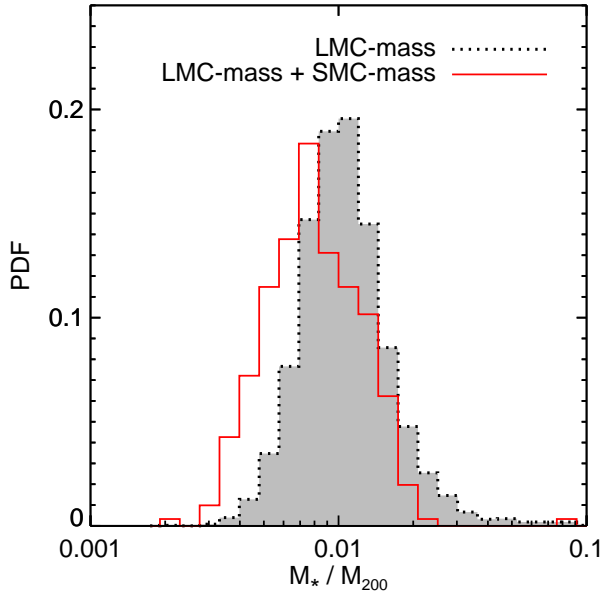


Figure 2. The distribution of stellar-to-halo mass ratios at $z = 0$ in the EAGLE simulation for *field* LMC-mass dwarfs. We show the distribution for all LMC-mass galaxies (dotted line) and for those that have an SMC-mass satellite (solid line). Having an SMC-mass satellite biases the LMC-mass dwarfs towards 1.3 times higher halo masses.

LMC-mass dwarfs is larger than for more massive galaxies, but is significantly smaller than for lower mass dwarfs (Sawala et al. 2015). For LMC-mass galaxies, a large fraction of the scatter is due to haloes having different concentrations and binding energies (Matthee et al. 2017). Higher concentration objects, which typically formed earlier, have more time to form stars and experience less efficient feedback since they are more tightly bound.

We further study the stellar-to-halo mass ratio, M_*/M_{200} , in Fig. 2, where we present the probability distribution function (PDF) of M_*/M_{200} for LMC-mass field dwarfs. The distribution is peaked at a value of $1.03^{+0.50}_{-0.31} \times 10^{-2}$ (68% confidence limit), with a sharp drop-off on both sides; this is in agreement with results from SDSS abundance matching models, although the dispersion of the distribution is larger than the 0.15 – 0.20 dex scatter typically assumed in these models (Moster et al. 2010; Guo et al. 2010).

Both the LMC and M33 are predicted to have been accreted recently (Patel et al. 2017), 1.5 and 0.4 Gyrs ago, respectively. We can assume that their halo masses at infall are likely similar to their present day masses, under the assumption that they are not significantly tidally stripped. Also, both galaxies are unlikely to have increased their stellar masses by more than 10% since infall, so their infall stellar masses roughly correspond to their present day masses. Finally, for the same LMC-mass galaxy selection criteria, EAGLE predicts the same M_*/M_{200} ratio for centrals at a slightly higher redshift, e.g. $z = 0.2$. Thus, we can use the M_*/M_{200} distribution in EAGLE to estimate the LMC halo mass at infall. Taking an LMC stellar mass of $2.7 \times 10^9 M_\odot$ (van der Marel & et al., 2002), we estimate the LMC total mass to be $2.6^{+1.1}_{-0.9} \times 10^{11} M_\odot$ (68% confidence limit), which is in agreement with the dynamical mass estimates of $2.5 \pm 0.8 \times 10^{11} M_\odot$ by Peñarrubia et al. (2016). M33 has a similar stellar mass, $3.0 \times 10^9 M_\odot$ (McConnachie 2012), and thus is expected to reside in a similar mass halo.

Observations indicate that the two brightest MW satellites, the LMC and SMC, were accreted as part of the same group. Does this observation bias the LMC mass estimates? To answer this ques-

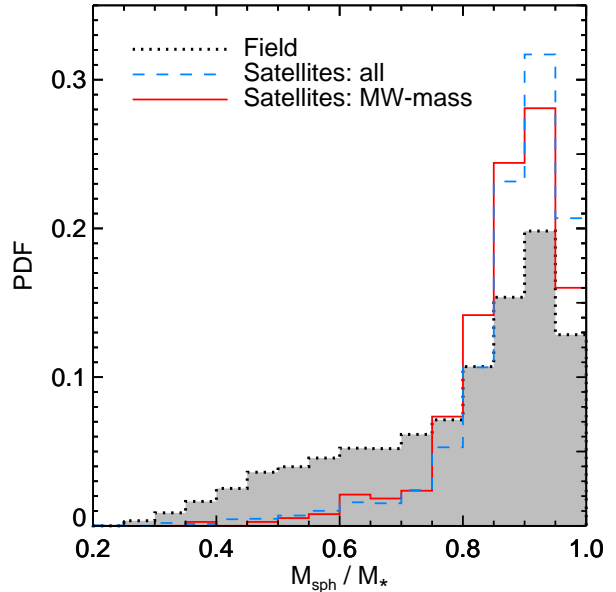


Figure 3. The morphology distribution of LMC-mass dwarfs. The morphology, defined as the ratio of the spheroid-to-total stellar mass within twice the half mass radius, is calculated by a dynamical decomposition into two components: disc and spheroid. The three lines show the distribution for LMC-mass dwarfs in the field (dotted line) and for satellites around all hosts (dashed line) and around MW-mass hosts (solid line).

tion, we proceed by identifying field LMC-mass galaxies that have an SMC-mass satellite. The SMC has a stellar mass roughly one third of the LMC (McConnachie 2012), so we define SMC-mass satellites as any objects with a stellar mass ~ 0.2 times or higher than that of its central LMC-mass galaxy. The binary LMC-SMC analogues reside in significantly more massive haloes for their stellar mass (see dashed curve in Fig. 2), with this sample having $M_*/M_{200} = 0.79^{+0.45}_{-0.27} \times 10^{-2}$ (68% confidence limit). Thus, the LMC halo is a factor of 1.3 times more massive than that of the typical LMC-mass dwarf and likely contributes a significant fraction of the mass of the MW halo ($\sim 20 - 40\%$ for a MW halo mass of $1 \times 10^{12} M_\odot$).

3.2 Morphology

Fig. 3 shows the distribution of the spheroid-to-total stellar mass ratio, M_{sph}/M_* , from a kinematic decomposition of each LMC-mass galaxy into bulge and disc components, as described in Section 2.2. Most of the field LMC-mass objects are bulge dominated; over 60% of the sample have $M_{\text{sph}}/M_* > 0.8$, which indicates that these galaxies are typically spherical and are velocity dispersion supported. A significant fraction ($\sim 20\%$) of field dwarfs have $M_{\text{sph}}/M_* < 0.6$, which indicates that they have significant ordered rotation. In contrast, there are very few LMC-mass satellites (3%) that show a disc-like morphology; most objects have $M_{\text{sph}}/M_* \approx 0.9$, and are thus largely dominated by their bulge. This is in qualitative agreement with visually classified morphologies in observations, where the fraction of early type galaxies increases in denser environments (Dressler 1980; Postman & Geller 1984; Bamford et al. 2009).

The morphology distribution of LMC-mass satellites around MW-mass haloes is very similar to that of satellites around all hosts. As we show later in Fig. 13, roughly half of the LMC-mass satellites of MW-mass haloes were accreted recently (< 3.5 Gyrs), and thus the lack of disc-like morphologies in LMC-mass satellites,

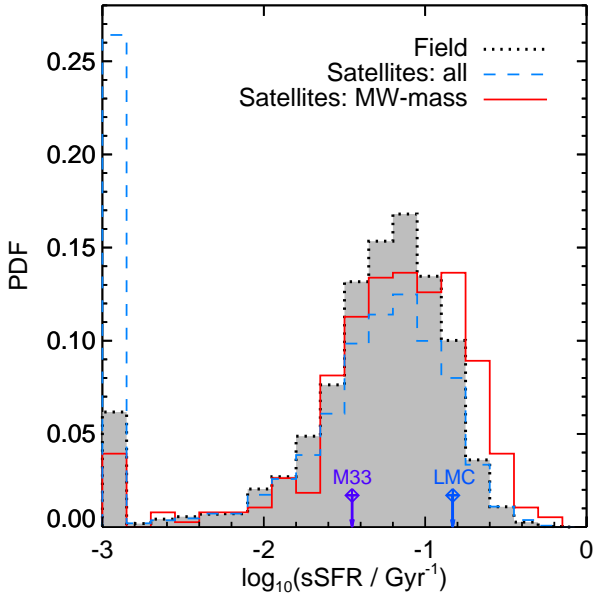


Figure 4. The specific star formation rate (sSFR) distribution of LMC-mass dwarfs. The lines correspond to dwarfs identified in the field (dotted), satellites around all hosts (dashed) and satellites around MW-mass haloes (solid). The galaxies that have zero or extremely small sSFR are all grouped together in the left-most bin. The two vertical arrows indicate the observed values for the LMC and M33 satellite galaxies.

compared to their field counterparts, is puzzling. It suggests that in EAGLE, once some of the galaxies become a satellites, they undergo a rapid morphological transformation. The lack of disk satellites is also puzzling when comparing to observations, which find a larger fraction of late-type galaxies (e.g. Bamford et al. 2009). A similar discrepancy is present when comparing with the two Local Group satellites, the LMC and M33, which have disc-like morphologies. M33 is visually classified as a disc and the LMC, while visually classified as an irregular galaxy, is kinematically dominated by ordered rotation more akin to that of a disc galaxy (van der Marel & et al., 2002). The differences in the morphologies of dwarf galaxies between EAGLE and observations are unlikely to be due to resolution effects: LMC-mass dwarfs in EAGLE are resolved with ~ 1000 particles. To verify this we compared the morphology of LMC-mass dwarfs in two simulations from the EAGLE project (with side-length 25 Mpc), one at the fiducial resolution and the other at 8 times better mass resolution; the distribution of spheroid-to-total stellar mass ratios are approximately the same in the two simulations. Furthermore, Benítez-Llambay et al. (2018) demonstrated that the galaxy formation model employed in EAGLE is able to reproduce adequately the structure of disc-like galaxies. We note that a direct comparison of our results to observations is difficult because the disc/spheroid kinematic decomposition we use in the simulations differs from the customary photometry-based methods used in observational studies. Indeed, the correspondence between these two methods has significant scatter, and photometric decomposition methods tend to estimate lower bulge-to-total ratios, especially for low mass galaxies (Abadi et al. 2003; Okamoto et al. 2005; Scannapieco & et al., 2010; Bottrell et al. 2017).

3.3 Star formation rate

The distribution of specific SFR (sSFR), \dot{M}_*/M_* , of EAGLE LMC-mass galaxies is given in Fig. 4. The figure shows the well known sSFR bimodality (e.g. Wijesinghe et al. 2012), with a mode that

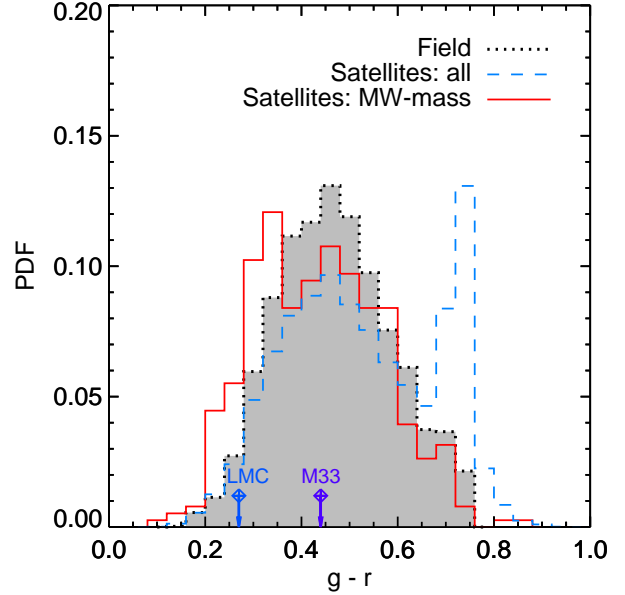


Figure 5. The distribution of $g - r$ colour for LMC-mass dwarfs found in the field (dotted), satellites around all hosts (dashed) and satellites around MW-mass host haloes (solid).

consists of star-forming galaxies with $\text{sSFR} \sim 0.06 M_{\odot} \text{yr}^{-1}$ and a second subsample of quiescent galaxies with none, or very little, ongoing star formation. Quantitatively, the sSFR of star-forming galaxies is a factor of two below observed values (e.g. the GAMA sample of Bauer et al. 2013), which is due to the overall SFRs at $z = 0$ in EAGLE being too low (for a more detailed analysis see Furlong et al. 2015). However, this does not affect our conclusions since our goal is to compare the differences between various dwarf galaxy samples. The fraction of quiescent dwarfs becomes most pronounced for the sample of satellites around all hosts and is a manifestation of the star formation quenching processes acting on satellite galaxies. For the star-forming population, the distribution of sSFR for the field and all-satellite samples is roughly the same, except for the normalization, in agreement with observational studies (Wijesinghe et al. 2012). It suggests that once quenching starts, it is a rapid process with a short time interval between the stage of forming stars like a field galaxy and becoming fully quiescent. This fits with the expectation that “strangulation”, the process of halting the supply of cold gas, is the main quenching process (Cole et al. 2000; Peng et al. 2015).

It is worth noting that satellite galaxies are not always quenched, and, at least for some time, their star formation can even be *enhanced*. This is clearly seen in the sample of LMC-mass satellites around MW-mass haloes, which has a smaller fraction of quiescent objects and for which the sSFR distribution of the star-forming sample is shifted towards higher values. Indeed, enhanced star formation may currently be taking place in the LMC, whose current SFR is twice its mean value over the last 2 Gyrs (Harris & Zaritsky 2009).

3.4 Colours

Fig. 5 presents the distribution of $g - r$ colours for our sample of LMC-mass dwarfs. While the field galaxies are well characterized by a unimodal distribution, the all-satellite sample is bimodal, with a subgroup of blue dwarfs peaking at $g - r = 0.45$, and a subgroup of red dwarfs peaking at $g - r = 0.75$. The EAGLE distribution of intrinsic colours is a good match to observations (e.g.

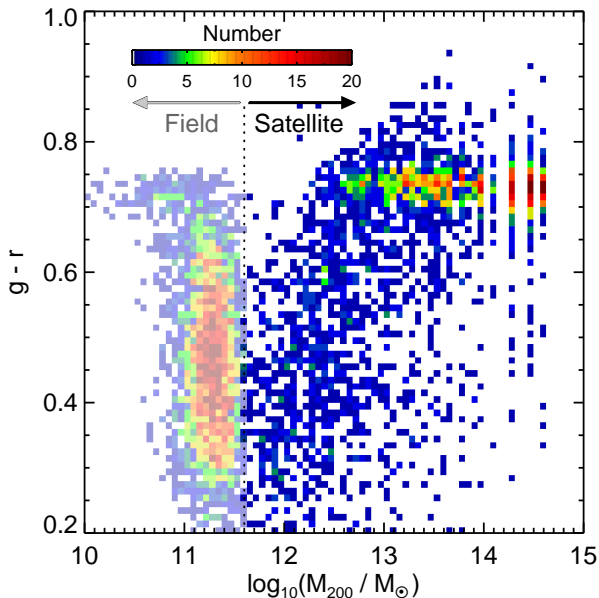


Figure 6. The distribution of $g-r$ colour for LMC-mass dwarfs as a function of halo mass. For field galaxies, the halo mass is that of their own halo and corresponds to the region left of the vertical dotted line. For satellite galaxies, the halo mass corresponds to that of their host haloes. The dotted vertical line at $M_{200} = 10^{11.6} M_{\odot}$ approximately separates the field from the satellite population.

see Taylor et al. 2015), and is an even better match when using a dust obscuration model that depends on gas fraction and metallicity (here we use the no-dust model; for details see Trayford et al. 2015). The LMC-mass satellites around MW-mass haloes have bluer colours than both the field and the all-satellites samples, and, furthermore, do not show a second “red” peak. As we will discuss shortly, the subgroup of red dwarfs mainly consists of satellites of rich groups and clusters, with $M_{200} > 1 \times 10^{13}$.

The LMC has a colour $(g-r)_{\text{LMC}} = 0.27$ (Eskew & Zaritsky 2011), which puts it in the tail of the field and all-satellites colour distribution (for a comparison with the $g-r$ distribution in observations, see Tollerud et al. 2011). However, when compared to the colour distribution of satellites around MW-mass hosts, the LMC is no longer an outlier (10% of EAGLE satellites are bluer than the LMC). M33 has a slightly redder colour, with $(g-r)_{\text{M33}} = 0.44$ (Tollerud et al. 2011), which is typical of a field galaxy that has been recently accreted onto the M31 halo (Patel et al. 2017).

3.5 Dependence on host halo mass

In order to understand the processes that shape the colour distribution of LMC-mass galaxies, we now explore the dependence on host halo mass. Fig. 6 shows the $g-r$ colour as a function of the halo mass for centrals and of the host halo mass for satellites. Most field LMC-mass dwarfs have $M_{200} < 10^{11.6} M_{\odot}$, and this mass threshold is shown as the dotted vertical line in the figure. The LMC-mass centrals can be broadly divided into two categories. First, there are the objects with $M_{200} < 10^{10.6} M_{\odot}$. These have a very low halo mass for their stellar mass and mainly correspond to backplash galaxies (see discussion in Section 3.1). Tracing the merger tree of these objects reveals that all of them were, at some time in the past, part of a massive, $M_{200} > 10^{13} M_{\odot}$, host halo. Secondly, there is the main population of LMC-mass galaxies, characterized by halo masses, $10^{10.7} M_{\odot} < M_{200} < 10^{11.6} M_{\odot}$. While these galaxies are predominantly blue, with a broad peak at

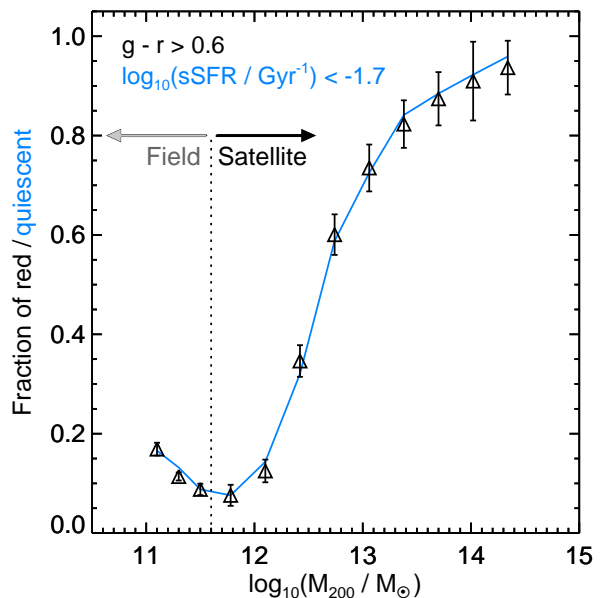


Figure 7. The fraction of red / quiescent LMC-mass dwarfs as a function of halo mass. The vertical dotted line separates the field galaxies (to the left) from the satellites (to the right). For field galaxies, the halo mass is that of their own halo, while for satellites, the halo mass is that of their host haloes. The symbols show the red fraction defined as galaxies with $g-r > 0.6$. The line shows the quiescent fraction defined as dwarfs with $\log(\text{sSFR}/\text{Gyr}^{-1}) < -1.7$. The error bars represent the 1σ bootstrap uncertainties and are roughly the same for both fractions.

$g-r = 0.45$, the distribution has a red tail, with a 15% fraction of red, $g-r > 0.6$, central galaxies (see Fig. 7). This population of passive central galaxies could be the result of self-quenching or mostly consist of backlash galaxies. To identify the main process, we followed the merger tree of all red LMC-mass centrals to identify the fraction that were satellites at any point during their formation history. We find that at most 35% of them were satellites in the past, suggesting that the dominant process for producing LMC-mass red centrals is self-quenching.

The colour distribution of LMC-mass satellites shows a distinct trend with the mass of their host halo. Due to the limited volume of EAGLE, there are only a few haloes more massive than $10^{14} M_{\odot}$ and each vertical strip at those masses corresponds to the satellites in each of those hosts. Note that the average number of LMC-mass satellites per host varies strongly with their host halo mass. A cluster with $M_{200} \sim 10^{14}$ has on average around 30 LMC-mass dwarfs, whereas only 1 out of 5 haloes with $M_{200} \sim 10^{12}$ has an LMC-mass dwarf. With a few exceptions, there are hardly any red satellites in haloes with $M_{200} < 10^{12} M_{\odot}$, and most satellites of $\sim 10^{12} M_{\odot}$ haloes are blue (defined as $g-r < 0.6$). The fraction of red satellites rapidly increases with higher host mass, with red LMC-mass dwarfs becoming dominant in hosts more massive than $10^{12.6} M_{\odot}$ (see also Fig. 7).

To quantify how many LMC-mass dwarfs are passive, we split the population into red and blue galaxies, according to whether $g-r > 0.6$ or $g-r < 0.6$, respectively. The fraction of red galaxies as a function of host halo mass is shown in Fig. 7 and, as Fig. 6, it combines in one plot both field and satellite galaxies. We find that few field galaxies are red ($\sim 15\%$ on average) and that the field red fraction shows a small, but statistically significant, trend with halo mass: an LMC-mass dwarf is slightly more likely to be red if it resides in a lower mass halo. This trend is driven by backplash galaxies, which, on average, are both redder and, due to

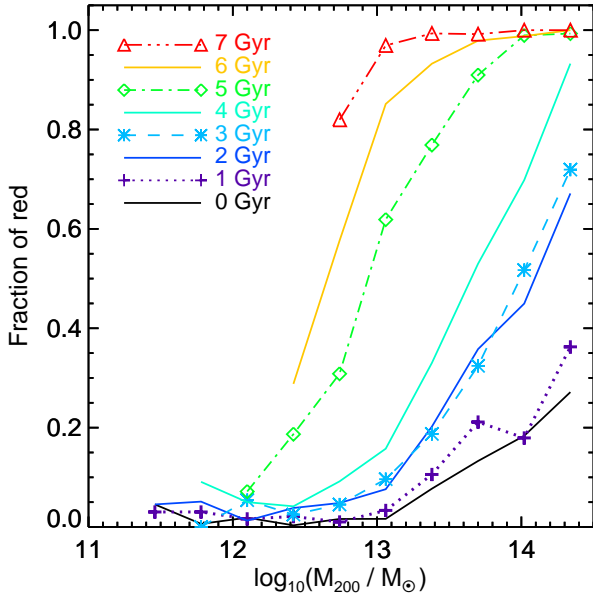


Figure 8. The fraction of red LMC-mass satellites as a function of their host halo mass. The curves show the red fraction at various times after infall into the host halo, with $t = 0$ corresponding to the time of infall. The fraction is shown only for M_{200} bins with 10 or more LMC-mass dwarfs. Thus, lines corresponding to infall times of 6 Gyrs or more do not extend down to low M_{200} values ($\lesssim 10^{12.5} M_{\odot}$).

tidal stripping, have lower halo masses. Interestingly, the fraction of red galaxies does not show any discontinuity as halo mass increases and we switch from centrals to satellites in low mass hosts. Furthermore, this transition region is where we find the smallest fraction of red dwarfs. As the host halo mass increases, we find a larger fraction of red satellites, with most ($\sim 90\%$) of LMC-mass galaxies in clusters ($M_{200} > 10^{14} M_{\odot}$) having red colours.

Fig. 7 also shows the fraction of quiescent galaxies, which are defined as those with specific star formation rates, $sSFR < 0.02/\text{Gyr}$. The quiescent fraction is roughly equal to the red fraction, and both show the exact same dependence on mass. While most quiescent dwarfs have red colours, this is not the case for every galaxy, with some having low $sSFR$ and blue colours and vice versa. This is due to the $sSFR$ being a measure of instantaneous star formation, while the colour is sensitive to the integrated recent star-formation history.

The results presented in Fig. 7 are consistent with observations, which report that it is extremely rare to find field dwarfs with no active star formation (e.g. Geha et al. 2012). The observations also support the trend with host halo mass: most LMC-mass satellites around faint centrals are blue, whereas most satellites in rich groups and clusters are red (e.g. Weinmann et al. 2006; Wang & et al., 2014; Sales et al. 2015; Geha et al. 2017; Wang et al. 2018).

Fig. 8 presents the fraction of red satellites at various times after infall as a function of their host halo mass. At infall, which corresponds to $t = 0$ Gyrs in the figure, most LMC-mass satellites are blue; the only exception are the high mass haloes, $M_{200} > 10^{13} M_{\odot}$, which accrete a non-negligible fraction of red dwarfs. Most of these dwarfs correspond to preprocessed satellites, which, before falling into their $z = 0$ host, were satellites of another halo (McGee et al. 2009; Wetzel et al. 2013; Hou et al. 2014). Higher mass haloes accrete, on average, more haloes with $M_{200} \gtrsim 10^{12} M_{\odot}$, which can host LMC-mass satellites themselves, and thus accrete more preprocessed LMC-mass dwarfs.

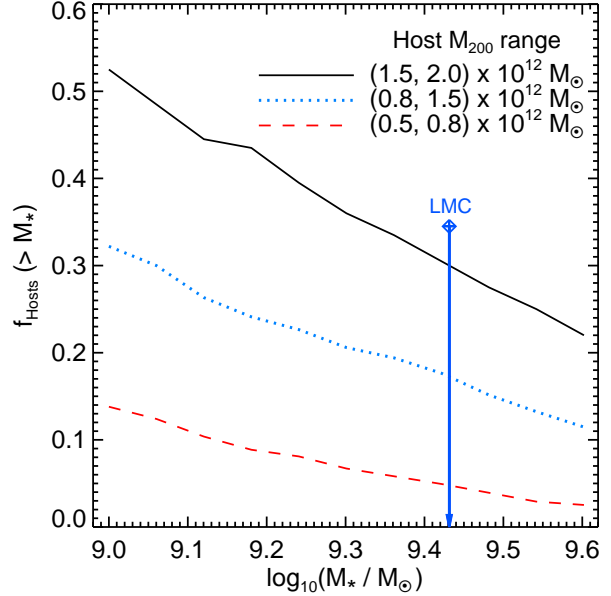


Figure 9. The fraction of hosts that have at least one LMC-mass satellite dwarf as a function of the stellar mass, M_* , of the satellite. The various lines correspond to different host halo masses: $0.5 - 0.8$ (dashed), $0.8 - 1.5$ (dotted) and $1.5 - 2.0 \times 10^{12} M_{\odot}$ (solid). Satellites are defined as galaxies within a distance, R_{50} , from a more massive halo. The vertical arrow indicates the van der Marel & et al., (2002) LMC stellar mass estimate of $2.7 \times 10^9 M_{\odot}$.

The results shown in Fig. 8 can be used to estimate the quenching timescale for LMC-mass dwarfs as a function of their host halo mass. For this, we follow, at fixed halo mass, the change in the red fraction as a function of time after infall. Hosts with masses, $M_{200} \sim 10^{12} M_{\odot}$, have a very slowly increasing red fraction such that, even 5 Gyrs after infall, only $\sim 5\%$ of LMC-mass satellites are red. Thus, these hosts have very long timescales for quenching LMC-mass dwarfs. This is in good agreement with SDSS observations that predict quenching timescales larger than 9 Gyrs (Wheeler et al. 2014), and with the trends observed in the Local Group, where the quenching time increases rapidly with the satellite stellar mass (Wetzel et al. 2015; Fillingham et al. 2015; Simpson et al. 2018). These long quenching times suggest that starvation is the main quenching process, with satellites not being able to accrete new gas. For example, the LMC had an average SFR of $0.2 M_{\odot} \text{ yr}^{-1}$ over the past 2 Gyrs and, given that it has an HI gas mass of at least $0.5 \times 10^9 M_{\odot}$, it can keep forming stars at the same rate for at least another 2.5 Gyrs. By then, the LMC would have orbited the MW for about 4 Gyrs, which is around the time when it will merge with the MW (Cautun et al. 2018).

For hosts more massive than the MW, the quenching timescales decrease rapidly. For example, half of the LMC-mass satellites of hosts with masses, $M_{200} \sim 10^{13} M_{\odot}$, are already red 5 Gyrs after infall. For cluster mass haloes, $M_{200} \sim 10^{14} M_{\odot}$, the quenching is even more rapid, with half of their dwarfs being red 2 – 3 Gyrs after infall. This is in agreement with the SDSS based quenching timescales derived by Wetzel et al. (2013), who also found that quenching progresses faster in more massive haloes. This indicates that the dominant quenching process varies with host halo mass, from starvation in the case of MW-mass hosts to ram pressure stripping for cluster mass hosts. The latter process becomes important when ram pressure, which depends on the satellite velocity and gas density of the host halo, overcomes the restoring gravitational force generated by the satellite’s mass distribution

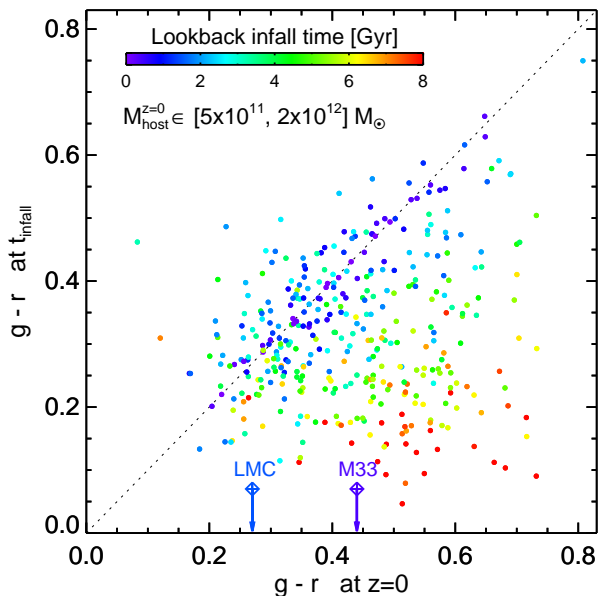


Figure 10. The colour evolution of LMC-mass dwarfs that are satellites of MW-mass haloes. We show the $g-r$ colour at infall versus the $g-r$ colour at $z=0$. Each symbol corresponds to an LMC-mass satellite, with the colour indicating the lookback time to infall (see legend). The two vertical arrows show the present-day colours of the LMC and M33 and the arrows are coloured according to the estimated infall time of the satellites.

(McCarthy et al. 2008). In MW-mass haloes ram pressure does not overcome the gravitational restoring force of LMC-mass dwarfs (Simpson et al. 2018), but ram pressure increases rapidly with host halo mass, since the satellites of more massive hosts are moving more rapidly inside a denser gas medium.

4 LMC-MASS DWARFS IN MW-MASS HOSTS

In this section we investigate in more detail the properties and evolution of LMC-mass satellites around MW-mass host haloes. In particular, we investigate differences between infall time, pericenter and evolution of red and blue LMC-mass dwarfs, and relate these properties to the brightest Galactic satellite, the LMC.

4.1 Abundance

We first study the abundance of LMC-mass dwarfs around MW-mass haloes. As discussed in Section 2, we found 381 EAGLE LMC-mass satellite galaxies residing in MW-mass hosts with masses in the range, $M_{200} \in [0.5, 2] \times 10^{12} M_{\odot}$. We split this sample into three subsets according to the host halo mass, and for each subset we calculate the fraction of hosts that have at least one LMC-mass satellite as a function of the satellite’s stellar mass. The outcome is shown in Fig. 9. The probability of finding a massive dwarf depends primarily on the host halo mass, and, for a fixed host halo mass, it decreases with increasing stellar mass of the satellite (Boylan-Kolchin et al. 2011; Busha et al. 2011; Cautun et al. 2014).

Satellite dwarfs with a stellar mass of $2.7 \times 10^9 M_{\odot}$, which corresponds to the LMC, are very rare (4%) in haloes with $M_{200} \in [0.5, 0.8] \times 10^{12} M_{\odot}$ and somewhat more common (16%) in haloes with $M_{200} \in [0.8, 1.5] \times 10^{12} M_{\odot}$, in agreement with previous theoretical and observational studies (e.g. Boylan-Kolchin et al. 2011; Robotham et al. 2012; Guo et al. 2013). The presence of such a massive satellite around the MW imposes a lower limit on the MW

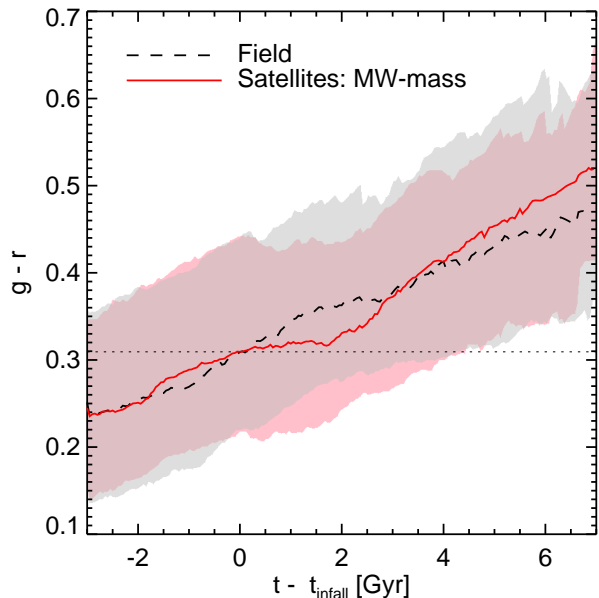


Figure 11. The evolution of the colour distribution for two samples of LMC-mass dwarfs: satellites of MW-mass hosts (in red) and a control sample of field galaxies (in black). The latter was obtained by pairing each satellite at infall with a field dwarf of the same colour. The evolution is expressed as a function of time after infall for each satellite galaxy, with infall time defined as $t = 0$, and $t < 0$ and $t > 0$ corresponding to before and after infall respectively. The dashed and solid lines correspond to the medians of the two distributions, while the shaded regions show the 16th and 84th percentiles. The dotted horizontal line is shown for reference, and corresponds to the median colour value at $t = 0$.

halo mass, such that masses as low as $M_{200} \sim 0.5 \times 10^{12} M_{\odot}$ are unlikely. The most stringent constraint comes when the SMC is also included, which is itself unexpectedly massive, to suggest a MW halo mass larger than $1.0 \times 10^{12} M_{\odot}$ with 90% confidence (Cautun et al. 2014).

4.2 Colour evolution

We show in Fig. 12 the evolution of two LMC-mass galaxies which by $z = 0$ have become satellites of MW-mass haloes. The one shown on the left is analogous to our LMC: it has a very blue $g-r$ colour, is actively forming stars and it recently passed its first pericentre, having fallen into its host MW halo only 2 Gyrs ago. We contrast this blue dwarf with a red LMC-mass satellite, which is shown in the right panels of Fig. 12. The two examples offer the opportunity to highlight both similarities and differences between blue and red satellites. The discussion which follows is based on investigating a larger sample of LMC-mass satellites and summarizes the typical behaviour seen for the majority of objects (some of the properties are studied in more detail in later figures).

On average, red satellites have fallen in a longer time ago and, in many cases, had a smaller gas fraction at infall than blue satellites mostly due to self-quenching. The latter is not the case for the red dwarf shown in Fig. 12, which at infall had a similar gas fraction as the example blue dwarf. Once accreted, many satellites experience an episode of gas compression, which leads to increased star formation (Dressler & Gunn 1983; Zabludoff et al. 1996; Sabatini et al. 2005). This phenomenon has also been seen in cluster galaxies in the ILLUSTRIS simulation (Mistani et al. 2016), which has a different treatment of baryonic physics from EAGLE. This episode typically occurs in gas rich dwarfs shortly after entering the halo and,

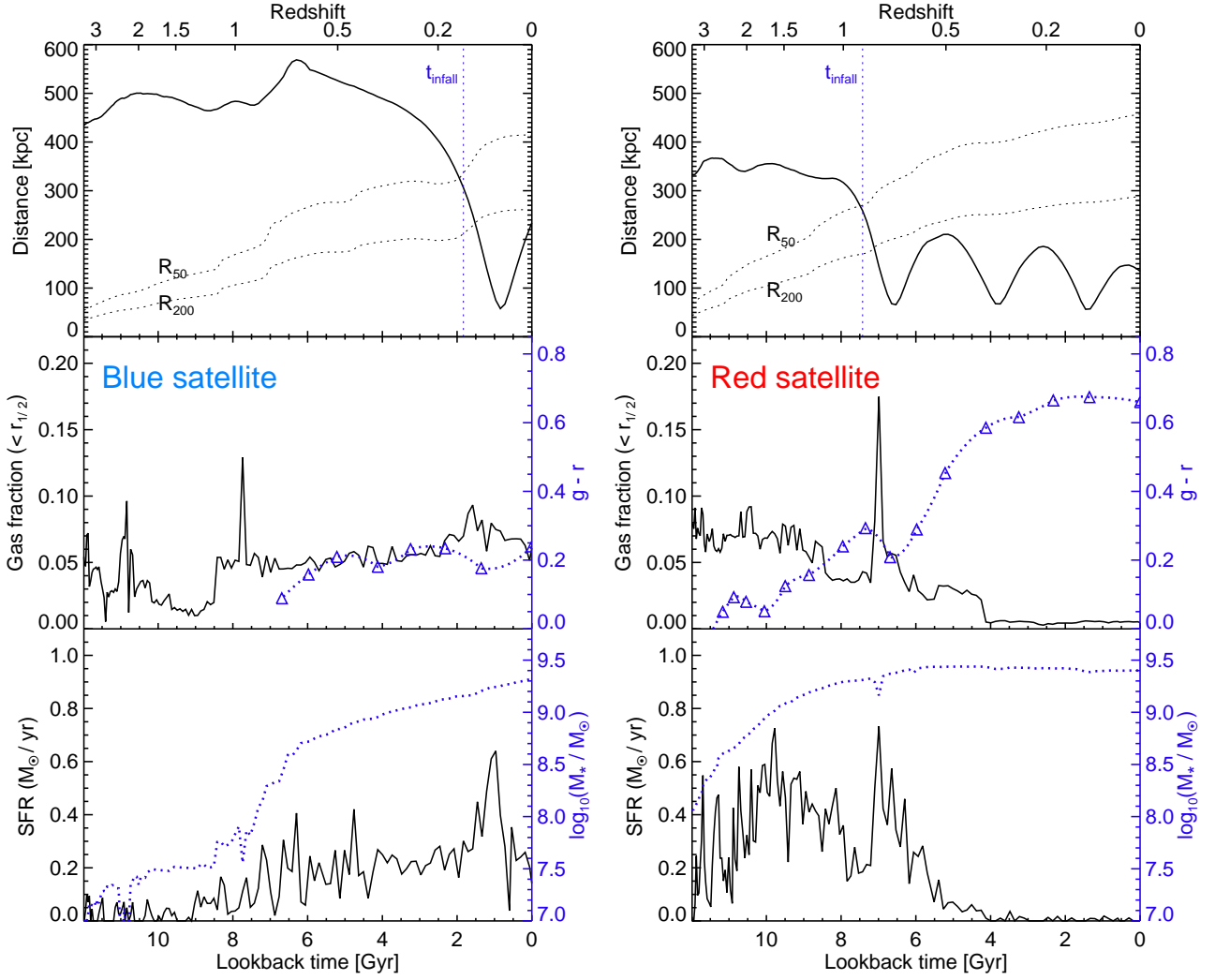


Figure 12. The formation history of two LMC-mass dwarfs which by the present have become satellites of two MW-mass haloes. The left and right columns show LMC-mass dwarfs that, at $z = 0$, have blue and red $g - r$ colours, respectively. *Top row:* the distance between the dwarf and its present day host halo, with dotted lines indicating the evolution of the host radii, R_{200} and R_{50} , and the vertical dashed line indicates the moment of infall into the MW-mass host. *Middle row:* the evolution of the LMC-mass dwarf’s gas fraction (left axis) and $g - r$ colour (right axis). Colours are available only for galaxies with $M_* > 5 \times 10^8 M_\odot$ and for a limited number of redshifts. *Bottom row:* the evolution of the LMC-mass dwarf SFR (left axis) and stellar mass (right axis).

in the examples shown in Fig. 12, it takes place at a lookback time of 1.5 and 7.0 Gyrs for the blue and red satellites, respectively. The typical gas compression is similar to that seen in the blue dwarf example, but there is also a significant fraction of the population that undergoes very strong gas compression similar to the one seen in the red dwarf example. This effect, enhanced star formation due to gas compression, is the reason why LMC-mass satellites in MW-mass hosts have, on average, both higher sSFR and blue colours than the field population (see Figs 4 and 5).

The two examples in Fig. 12 highlight another process that affects the evolution of dwarf galaxies: mergers with other dwarfs (Deason et al. 2014). Both dwarfs had at least one merger with another dwarf galaxy, which took place at a lookback time of 7 and 9 Gyrs for the blue and red LMC-mass analogues, respectively. The merger can be inferred from the small wiggles in the distance plot shown in the top panel of Fig. 12, which are due to the relative orbital motion of the merging dwarfs. For the blue satellite, the merging dwarf is massive and its disruption leads to a sudden increase in the stellar mass of the LMC-mass progenitor (see dashed line in the bottom-left hand panel of Fig. 12). The merger leads to rapid gas compression and enhanced star formation. In contrast, the progen-

itor of the red LMC-mass dwarf experiences a lower mass merger and its imprint on both the gas fraction and SFR is less pronounced, with possibly enhanced SFR around 10 Gyrs ago.

In order to understand the colour evolution of LMC-mass satellites better, we show the correlation between $g - r$ colour at infall and at the present time in Fig. 10. Each point corresponds to an LMC-mass satellite in a MW-mass host, with colour reflecting the lookback time to infall. At infall, most dwarfs are blue, i.e. $g - r < 0.6$, with only 4 out of the 381 dwarfs that are red. Many of the galaxies that fell in recently (< 2 Gyrs) have, on average, at $z = 0$, slightly bluer colours than at infall, which is due to the enhanced star formation that takes place in these dwarfs when they first enter a MW-mass host halo. In contrast, galaxies accreted between 3 to 6 Gyrs ago are significantly redder than at infall and have typically experienced a colour change $\Delta(g - r) \simeq 0.15$. Galaxies accreted more than 6 Gyrs ago show the largest reddening, corresponding to a colour change since infall of $\Delta(g - r) \simeq 0.3$ or higher. Interestingly, while the satellites accreted the earliest show the largest change in colour, they were, on average, very blue at infall and thus are not necessarily classified as red, i.e. as having $g - r > 0.6$. The red satellites have a large distribution of ac-

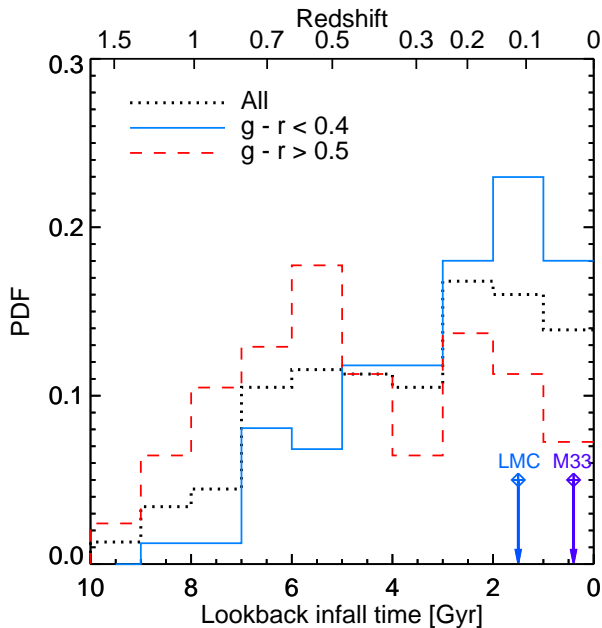


Figure 13. The distribution of infall times for the LMC-mass dwarfs that are satellites of MW-mass haloes. Shown are the distributions for the entire sample (dotted line) and for the sample split according to $z = 0$ colour: $g - r < 0.4$ (solid line) and $g - r > 0.5$ (dashed line). The two colour-selected subsamples correspond to roughly a third of the full sample. The two vertical arrows show the estimated infall times of the LMC and M33 (the M33 estimate is highly uncertain; see discussion in main text).

cretion ages, being a mixture of dwarfs accreted long ago, and recently accreted objects whose colour at infall was slightly bluer than $g - r = 0.6$.

The LMC is estimated to have been accreted into the MW about 1.5 Gyrs ago (Patel et al. 2017) and its very blue colour is consistent with this prediction. In contrast, the orbit of M33 is much more uncertain, with predicted infall times in the literature varying from 0.4 Gyrs (Patel et al. 2017) to more than 4 Gyrs (Putman et al. 2009; McConnachie et al. 2009). The former are based on proper motions for both M33 and M31, but an early accretion scenario only includes a small region of the allowed proper motion space. The latter use the warped HI disc (Putman et al. 2009) and the faint stellar structure surrounding M33 (McConnachie et al. 2009) as evidence of a past close encounter between M33 and M31, suggesting that M33 was accreted at least several Gyrs ago. The $g - r$ colour of M33 is unlikely to distinguish between the two scenarios (see Fig. 10), since its present day colour is consistent with both late and early accretion, with the latter option being acceptable if M33 was very blue when it fell into M31. Curiously, the M33 star formation history has a prominent peak around 2 Gyrs ago (Williams et al. 2009) that could correspond to enhanced star formation due to gas compression within ~ 1 Gyr after infall into M31 (see discussion of Fig. 12). This hypothesis would favour the early accretion scenario.

Fig. 11 contrasts the colour evolution of LMC-mass satellites around MW-mass haloes with that of similar dwarfs in the field. The latter were selected by assigning to each satellite at infall a field counterpart of the same colour. The figure shows the evolution from 3 Gyrs before infall to 7 Gyrs after infall. Before infall, we find a close match in the evolution of the satellite and field samples. Since these two samples were matched to have the same colours at infall, this indicates that MW-mass haloes do not affect the evolution of LMC-mass dwarfs outside R_{50} . After infall, for the next ~ 3 Gyrs, the satellites are bluer on average than they would have been had

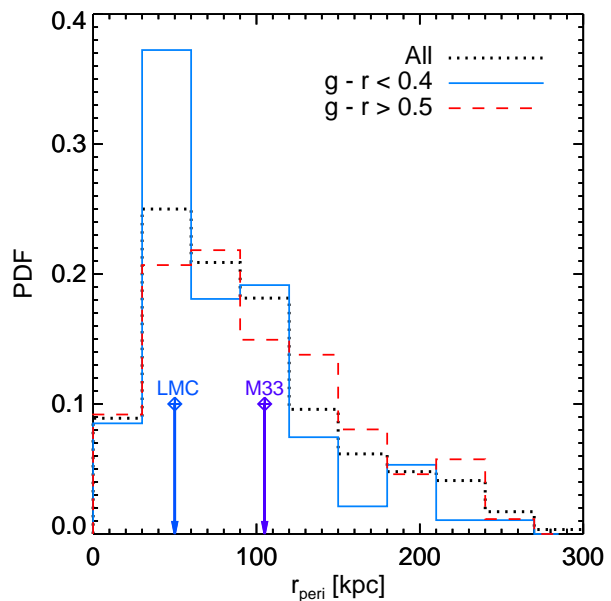


Figure 14. The distribution of first pericentric distances for LMC-mass dwarfs that are satellites of MW-mass haloes. As in Fig. 13, we show the full sample (dotted line) and $g - r$ colour selected subsamples: $g - r < 0.4$ (solid line) and $g - r > 0.5$ (dashed line). The two vertical arrows show the estimated first pericentre distance of the LMC and M33.

they stayed in the field. As we discussed above, this is due to the enhanced star formation triggered by gas compression. Interestingly, the colour of the satellites remains the same for up to 2 Gyrs after infall, after which it starts to redden faster than in their field counterparts. By 6 Gyrs, the satellites are $\Delta(g - r) \simeq 0.2$ redder than at infall, and $\Delta(g - r) \simeq 0.05$ redder than if they would have remained in the field.

The two examples in Fig. 12, as well as Fig. 10, showcase the importance of infall time: early accreted dwarfs are redder than late accreted ones. To study the dependence between infall time and the present day $g - r$ colour statistically, we split the LMC-mass satellites of MW-mass haloes into two subsets according to their $z = 0$ colour: the reddest third, corresponding to $g - r > 0.5$, and the bluest third, where $g - r < 0.4$. As the name suggests, each subset contains roughly one third of the full sample. Fig. 13 shows the distribution of lookback times to infall for these two subsets, with $t = 0$ corresponding to the present day. We find a strong trend of the present day colour with infall time, with the reddest third subset having earlier infall times on average. In contrast, the bluest third subset was generally accreted more recently, with most objects having fallen into their MW hosts less than 7 Gyrs ago.

It is intriguing to compare the infall time of LMC-mass satellites with that of lower mass satellites of MW-mass haloes. Shao et al. (2018) studied the distribution of infall times for the brightest 11 satellites of EAGLE MW-mass haloes to find that most such dwarfs were accreted between 8 and 10 Gyrs ago, with only 40% of objects having lookback times to infall below 7 Gyrs. In contrast, 50% of the LMC-mass satellites were accreted less than 3.5 Gyrs ago. Due to their higher total mass, LMC-mass dwarfs experience strong dynamical friction and thus sink towards the halo centre, where they end up being tidally disrupted and possibly merging with the central galaxy.

In Fig. 14 we investigate if the colour evolution of LMC-mass satellites depends on their orbit. We plot the distribution of first pericentre distances for all the sample, as well as for the bluest-third

and reddest-third subsets. The distribution peaks around ~ 50 kpc and drops sharply for smaller distances, while for distances larger than 50 kpc there is a more gradual decrease. We find a clear difference between the pericentre distances of the bluest-third and those of the reddest-third subset, with the former typically closer to the halo centre. This suggests that, on average, satellites that get close to the central galaxy are more likely to experience gas compression and thus form more stars.

Fig. 14 also shows the predicted LMC and M33 pericentres of 50 and 105 kpc, respectively (Patel et al. 2017). These measurements are in good agreement with the simulation predictions. In particular, the LMC pericentre is near the peak of the distribution. Interestingly, the McConnell et al. (2009) scenario of a close encounter between M33 and M31 in order to explain the warped HI disc and the extended stellar structure of M33, requires a pericentric passage of ~ 50 kpc; this value is favoured more by the EAGLE data than the ~ 100 kpc pericentre suggested by the M31 and M33 proper motions.

5 CONCLUSIONS

We have investigated the properties of LMC-mass dwarf galaxies in the main EAGLE cosmological hydrodynamics simulations of galaxy formation. By LMC-mass dwarfs we mean the population of galaxies in the simulation that have a stellar mass similar to the LMC, i.e. in the range $[1, 4] \times 10^9 M_{\odot}$. EAGLE is well suited to this study because of its rare combination of high resolution and large volume, and because it produces a population of galaxies with realistic masses, sizes, star formation rates, colours and gas content. To understand the effects of environment, the LMC-mass dwarfs were split into satellite and field galaxy samples. The former are dwarfs which are inside the halo of a brighter galaxy while the latter are central galaxies. In order to focus on objects similar to the LMC and M33, which are the brightest satellites of the MW and M31, respectively, we selected a further subset of LMC-mass satellites hosted by MW-mass haloes.

Our main conclusions are summarised as follows:

(i) Field LMC-mass dwarfs reside in haloes with $M_{200} \sim 2 \times 10^{11} M_{\odot}$ and have a stellar-to-halo mass ratio of $1.03_{-0.31}^{+0.50} \times 10^{-2}$, in agreement with abundance matching estimates (see Figs 1 and 2). Furthermore, LMC-mass centrals that have a SMC-mass satellite reside in haloes 1.3 times more massive than the typical LMC-mass dwarf. This suggests that the LMC halo mass at infall was relatively high; EAGLE predicts $M_{200} = 3.4_{-1.2}^{+1.8} \times 10^{11} M_{\odot}$ (68% confidence interval).

(ii) In agreement with observations, the $g-r$ colour distribution is bimodal with the red mode consisting mainly of LMC-mass satellites of massive groups and clusters (see Fig. 5). Field galaxies have a unimodal colour distribution and are mostly blue; only 15% of them are red, i.e. they have $g-r > 0.6$. The quenching of field dwarfs is predominantly driven by self-quenching.

(iii) The fraction of satellites that are red increases rapidly with host mass, from 10% for MW-mass hosts, to 50% for hosts with $M_{200} = 5 \times 10^{12}$, and then to over 90% for hosts with $M_{200} > 3 \times 10^{13}$ (see Fig. 7).

(iv) The quenching timescale, defined as the time after infall when half of the satellites have acquired red colours, varies strongly with host halo mass, with values of >5 , 5 and 2.5 Gyrs for hosts with masses, $M_{200} \sim 10^{12}$, 10^{13} and $10^{14} M_{\odot}$, respectively (Fig. 8). It indicates that the dominant quenching process varies with host halo mass, from starvation in the case of MW-mass hosts

to ram pressure stripping for clusters.

(v) LMC-mass satellites hosted by MW-mass haloes show enhanced star formation and bluer $g-r$ colours than both the field and the overall satellite population (see Figs 4 and 5). Shortly after accretion into the MW-mass host, the dwarfs experience gas compression that leads to an episode of increased star formation.

(vi) The prevalence of LMC-mass satellites in MW-mass haloes depends primarily on halo mass. The presence of the LMC in MW and M33 in M31 suggests that the two giant galaxies reside in haloes more massive than $\sim 10^{12} M_{\odot}$ (see Fig. 9).

(vii) After infall into MW-mass haloes, LMC-mass dwarfs have slightly bluer colours for ~ 2 Gyrs, after which they quickly redden, with on average $\Delta(g-r) = 0.2$ and 0.4 after 6 and 8 Gyrs from infall, respectively (see Fig. 10).

(viii) More than half of the LMC-mass satellites of MW-mass hosts were accreted less than 3.5 Gyrs and most ($\sim 70\%$) within the last 5 Gyrs (see Fig. 13). In contrast, less than 30% of satellites with similar mass to the classical MW dwarfs were accreted within the last 5 Gyrs (Shao et al. 2018).

One of the goals of this paper has been to understand better the processes that dominate the formation of LMC-mass dwarfs, with particular emphasis on the LMC and M33 galaxies. The orbit of M33 is not very well constrained because of large uncertainties in the proper motions of M33 and M31. Currently, the most likely scenario inferred from proper motion data is that M33 fell into the M31 halo only recently, ~ 0.4 Gyrs ago, and is on an elongated orbit with a first pericentre distance of 100 kpc (Patel et al. 2017). However, this seems inconsistent with the warped HI disc and the extended stellar distribution around M33, which could naturally be explained by a close encounter with M31, e.g. with a pericentre distance of ~ 50 kpc about 3 Gyrs ago (McConnell et al. 2009). Our results favour the second possibility because: 1) the enhanced star formation rate in M33 around 2 Gyrs ago, which we found to arise naturally from gas compression after infall into the larger halo; and 2) the higher likelihood of a pericentric distance of 50 kpc, which is twice as likely as the larger values expected in the very recent infall scenario.

The LMC, whose orbit is better constrained than the M33 one, is thought to have been accreted around 1.5 Gyrs ago (Patel et al. 2017) and both its current enhanced star formation and very blue colours can be explained by gas compression upon entry, which we found to be common among the recently accreted satellites of MW-mass haloes. The distribution of infall times suggest that LMC-mass satellites of MW-mass haloes have short lifetimes, with dynamical friction rapidly causing their orbit to decay towards their host centre.

ACKNOWLEDGEMENTS

We thank the anonymous referee for detailed comments that have helped us improve the paper. SS, MC and CSF were supported by the Science and Technology Facilities Council (STFC) [grant number ST/F001166/1, ST/I00162X/1, ST/P000541/1]. AD is supported by a Royal Society University Research Fellowship. This work used the DiRAC Data Centric system at Durham University, operated by ICC on behalf of the STFC DiRAC HPC Facility (www.dirac.ac.uk). This equipment was funded by BIS National E-infrastructure capital grant ST/K00042X/1, STFC capital grant ST/H008519/1, and STFC DiRAC Operations grant ST/K003267/1 and Durham University. DiRAC is part of the National E-Infrastructure.

REFERENCES

- Abadi M. G., Navarro J. F., Steinmetz M., Eke V. R., 2003, *ApJ*, **591**, 499
- Bahé Y. M., et al., 2017, *MNRAS*, **470**, 4186
- Bamford S. P., et al., 2009, *MNRAS*, **393**, 1324
- Bauer A. E., et al., 2013, *MNRAS*, **434**, 209
- Benítez-Llambay A., Navarro J. F., Frenk C. S., Ludlow A. D., 2018, *MNRAS*, **473**, 1019
- Benson A. J., 2010, *Phys. Rep.*, **495**, 33
- Blanton M. R., Moustakas J., 2009, *ARA&A*, **47**, 159
- Booth C. M., Schaye J., 2009, *MNRAS*, **398**, 53
- Bottrell C., Torrey P., Simard L., Ellison S. L., 2017, *MNRAS*, **467**, 2879
- Boylan-Kolchin M., Springel V., White S. D. M., Jenkins A., 2010, *MNRAS*, **406**, 896
- Boylan-Kolchin M., Besla G., Hernquist L., 2011, *MNRAS*, **414**, 1560
- Bruzual G., Charlot S., 2003, *MNRAS*, **344**, 1000
- Busha M. T., Wechsler R. H., Behroozi P. S., Gerke B. F., Klypin A. A., Primack J. R., 2011, *ApJ*, **743**, 117
- Cautun M., Frenk C. S., van de Weygaert R., Hellwing W. A., Jones B. J. T., 2014, *MNRAS*, **445**, 2049
- Cautun M., Deason A. J., Frenk C. S., McAlpine S., 2018, in prep.
- Chabrier G., 2003, *PASP*, **115**, 763
- Cole S., Lacey C. G., Baugh C. M., Frenk C. S., 2000, *MNRAS*, **319**, 168
- Crain R. A., McCarthy I. G., Frenk C. S., Theuns T., Schaye J., 2010, *MNRAS*, **407**, 1403
- Crain R. A., et al., 2015, *MNRAS*, **450**, 1937
- Dalla Vecchia C., Schaye J., 2012, *MNRAS*, **426**, 140
- Davis M., Efstathiou G., Frenk C. S., White S. D. M., 1985, *ApJ*, **292**, 371
- Deason A., Wetzel A., Garrison-Kimmel S., 2014, *ApJ*, **794**, 115
- Deason A. J., Wetzel A. R., Garrison-Kimmel S., Belokurov V., 2015, *MNRAS*, **453**, 3568
- Dolag K., Borgani S., Murante G., Springel V., 2009, *MNRAS*, **399**, 497
- Dressler A., 1980, *ApJS*, **42**, 565
- Dressler A., Gunn J. E., 1983, *ApJ*, **270**, 7
- Eskew M., Zaritsky D., 2011, *AJ*, **141**, 69
- Fattahi A., Navarro J. F., Frenk C. S., Oman K. A., Sawala T., Schaller M., 2018, *MNRAS*, **476**, 3816
- Fillingham S. P., Cooper M. C., Wheeler C., Garrison-Kimmel S., Boylan-Kolchin M., Bullock J. S., 2015, *MNRAS*, **454**, 2039
- Fillingham S. P., Cooper M. C., Pace A. B., Boylan-Kolchin M., Bullock J. S., Garrison-Kimmel S., Wheeler C., 2016, *MNRAS*, **463**, 1916
- Furlong M., et al., 2015, *MNRAS*, **450**, 4486
- Geha M., Blanton M. R., Yan R., Tinker J. L., 2012, *ApJ*, **757**, 85
- Geha M., et al., 2017, *ApJ*, **847**, 4
- Guo Q., White S., Li C., Boylan-Kolchin M., 2010, *MNRAS*, **404**, 1111
- Guo Q., Cole S., Eke V., Frenk C., 2011, *MNRAS*, **417**, 370
- Guo Q., Cole S., Eke V., Frenk C., Helly J., 2013, *MNRAS*, **434**, 1838
- Harris J., Zaritsky D., 2009, *AJ*, **138**, 1243
- Hopkins P. F., 2013, *MNRAS*, **428**, 2840
- Hou A., Parker L. C., Harris W. E., 2014, *MNRAS*, **442**, 406
- Jethwa P., Erkal D., Belokurov V., 2016, *MNRAS*, **461**, 2212
- Kallivayalil N., van der Marel R. P., Alcock C., Axelrod T., Cook K. H., Drake A. J., Geha M., 2006, *ApJ*, **638**, 772
- Kallivayalil N., van der Marel R. P., Besla G., Anderson J., Alcock C., 2013, *ApJ*, **764**, 161
- Kimm T., et al., 2009, *MNRAS*, **394**, 1131
- Lagos C. d. P., et al., 2015, *MNRAS*, **452**, 3815
- Laporte C. F. P., Gómez F. A., Besla G., Johnston K. V., Garavito-Camargo N., 2018, *MNRAS*, **473**, 1218
- Liu L., Gerke B. F., Wechsler R. H., Behroozi P. S., Busha M. T., 2011, *ApJ*, **733**, 62
- Matthee J., Schaye J., Crain R. A., Schaller M., Bower R., Theuns T., 2017, *MNRAS*, **465**, 2381
- McAlpine S., et al., 2016, *Astronomy and Computing*, **15**, 72
- McCarthy I. G., Frenk C. S., Font A. S., Lacey C. G., Bower R. G., Mitchell N. L., Balogh M. L., Theuns T., 2008, *MNRAS*, **383**, 593
- McConnachie A. W., 2012, *AJ*, **144**, 4
- McConnachie A. W., et al., 2009, *Nature*, **461**, 66
- McGee S. L., Balogh M. L., Bower R. G., Font A. S., McCarthy I. G., 2009, *MNRAS*, **400**, 937
- Mistani P. A., et al., 2016, *MNRAS*, **455**, 2323
- Moore B., Diemand J., Stadel J., 2004, in Diaferio A., ed., *IAU Colloq. 195: Outskirts of Galaxy Clusters: Intense Life in the Suburbs*. pp 513–518 ([arXiv:astro-ph/0406615](https://arxiv.org/abs/astro-ph/0406615)), doi:10.1017/S1743921304001127
- Moster B. P., Somerville R. S., Maulbetsch C., van den Bosch F. C., Macciò A. V., Naab T., Oser L., 2010, *ApJ*, **710**, 903
- Muñoz-Mateos J. C., Gil de Paz A., Boissier S., Zamorano J., Jarrett T., Gallego J., Madore B. F., 2007, *ApJ*, **658**, 1006
- Okamoto T., Eke V. R., Frenk C. S., 2005, *MNRAS*, **363**, 1299
- Patel E., Besla G., Sohn S. T., 2017, *MNRAS*, **464**, 3825
- Peñarrubia J., Gómez F. A., Besla G., Erkal D., Ma Y.-Z., 2016, *MNRAS*, **456**, L54
- Peng Y., Maiolino R., Cochrane R., 2015, *Nature*, **521**, 192
- Planck Collaboration XVI 2014, *A&A*, **571**, A16
- Postman M., Geller M. J., 1984, *ApJ*, **281**, 95
- Pozzetti L., et al., 2010, *A&A*, **523**, A13
- Putman M. E., et al., 2009, *ApJ*, **703**, 1486
- Robotham A. S. G., et al., 2012, *MNRAS*, **424**, 1448
- Rosas-Guevara Y. M., et al., 2015, *MNRAS*, **454**, 1038
- Sabatini S., Davies J., van Driel W., Baes M., Roberts S., Smith R., Linder S., O’Neil K., 2005, *MNRAS*, **357**, 819
- Sales L. V., et al., 2017, *MNRAS*, **465**, 1879
- Sales L. V., Navarro J. F., Theuns T., Schaye J., White S. D. M., Frenk C. S., Crain R. A., Dalla Vecchia C., 2012, *MNRAS*, **423**, 1544
- Sales L. V., et al., 2015, *MNRAS*, **447**, L6
- Sawala T., et al., 2015, *MNRAS*, **448**, 2941
- Scannapieco C., et al., 2009, *MNRAS*, **396**, 696
- Scannapieco C., et al., 2010, *MNRAS*, **407**, L41
- Schaller M., Dalla Vecchia C., Schaye J., Bower R. G., Theuns T., Crain R. A., Furlong M., McCarthy I. G., 2015, *MNRAS*, **454**, 2277
- Schaye J., 2004, *ApJ*, **609**, 667
- Schaye J., et al., 2015, *MNRAS*, **446**, 521
- Shao S., Cautun M., Frenk C. S., Grand R. J. J., Gómez F. A., Marinacci F., Simpson C. M., 2018, *MNRAS*, **476**, 1796
- Simpson C. M., Grand R. J. J., Gómez F. A., Marinacci F., Pakmor R., Springel V., Campbell D. J. R., Frenk C. S., 2018, *MNRAS*, **478**, 548
- Springel V., 2005, *MNRAS*, **364**, 1105
- Springel V., Yoshida N., White S. D. M., 2001, *New Astron.*, **6**, 79
- Springel V., Di Matteo T., Hernquist L., 2005, *MNRAS*, **361**, 776
- Strateva I., et al., 2001, *AJ*, **122**, 1861
- Taylor E. N., et al., 2015, *MNRAS*, **446**, 2144
- Tollerud E. J., Boylan-Kolchin M., Barton E. J., Bullock J. S., Trinh C. Q., 2011, *ApJ*, **738**, 102
- Trayford J. W., et al., 2015, *MNRAS*, **452**, 2879
- Wang W., White S. D. M., 2012, *MNRAS*, **424**, 2574
- Wang Y. O., et al., 2014, *ApJ*, **786**, 8
- Wang W., Han J., Cooper A. P., Cole S., Frenk C., Lowing B., 2015, *MNRAS*, **453**, 377
- Wang H., et al., 2018, *ApJ*, **852**, 31
- Weinmann S. M., van den Bosch F. C., Yang X., Mo H. J., Croton D. J., Moore B., 2006, *MNRAS*, **372**, 1161
- Wetzel A. R., Tinker J. L., Conroy C., van den Bosch F. C., 2013, *MNRAS*, **432**, 336
- Wetzel A. R., Tollerud E. J., Weisz D. R., 2015, *ApJ*, **808**, L27
- Wheeler C., Phillips J. I., Cooper M. C., Boylan-Kolchin M., Bullock J. S., 2014, *MNRAS*, **442**, 1396
- Wiersma R. P. C., Schaye J., Smith B. D., 2009a, *MNRAS*, **393**, 99
- Wiersma R. P. C., Schaye J., Theuns T., Dalla Vecchia C., Tornatore L., 2009b, *MNRAS*, **399**, 574
- Wijesinghe D. B., et al., 2012, *MNRAS*, **423**, 3679
- Williams B. F., Dalcanton J. J., Dolphin A. E., Holtzman J., Sarajedini A., 2009, *ApJ*, **695**, L15
- Woods D. F., Geller M. J., 2007, *AJ*, **134**, 527
- Zabludoff A. I., Zaritsky D., Lin H., Tucker D., Hashimoto Y., Shectman S. A., Oemler A., Kirshner R. P., 1996, *ApJ*, **466**, 104
- van der Marel R. P., et al., 2002, *AJ*, **124**, 2639